

George E. Totten,¹ Luiz C. Casteletti,² Frederico A. P. Fernandes,³
and Juno Gallego⁴

Microstructural Characterization of Layers Produced by Plasma Nitriding on Austenitic and Superaustenitic Stainless Steel Grades

High chromium content is responsible for the formation of a protective passive surface layer on austenitic stainless steels (ASS). Due to their larger amounts of chromium, superaustenitic stainless steels (SASS) can be chosen for applications with higher corrosion resistance requirements. However, both of them present low hardness and wear resistance that has limited their use for mechanical parts fabrication. Plasma nitriding is a very effective surface treatment for producing harder and wear resistant surface layers on these steel grades, without harming their corrosion resistance if low processing temperatures are employed. In this work UNS S31600 and UNS S31254 SASS samples were plasma nitrided in temperatures from 400 °C to 500 °C for 5 h with 80 % H₂–20 % N₂ atmosphere at 600 Pa. Nitrided layers were analyzed by optical (OM) and transmission electron microscopy (TEM), x-ray diffraction (XRD), and Vickers microhardness testing. Observations made by optical microscopy showed that N-rich layers were uniform but their thicknesses increased with higher nitriding temperatures. XRD analyses showed that lower temperature layers are mainly composed by expanded austenite, a metastable nitrogen supersaturated phase with excellent corrosion and tribological properties. Samples nitrided at 400 °C produced a 5 μm thick expanded austenite layer. The nitrided layer reached 25 μm in specimens treated at 500 °C. There are indications that other phases are formed during higher temperature nitriding but XRD analysis was not able to determine that phases are iron and/or chromium nitrides, which are responsible for increasing hardness from 850 up to 1100 HV. In fact, observations made by TEM have indicated that formation of fine nitrides, virtually not identified by XRD technique, can begin at lower temperatures and their growth is affected by both thermodynamical and kinetics reasons.

KEYWORDS: plasma nitriding, expanded austenite, microstructure, XRD, TEM analysis

Introduction

Austenitic and superaustenitic stainless steels have extensively been applied in the production of corrosion resistant components. Nevertheless, their mechanical, tribological, and fatigue properties can be increased by thermochemical treatments as plasma nitriding [1–3]. At temperatures below 500 °C plasma nitriding of austenitic stainless steel can produce a nitrogen supersaturated metastable phase which is usually called “expanded austenite” or “S phase.” The mechanical, tribological, and fatigue properties of expanded austenite are very superior to those found in a white layer composed mainly by hard nitrides. Interstitial nitrogen atoms occupy disordered octahedral sites in the fcc crystal lattice of austenite, significantly increasing the lattice parameter due to very high (30–40 at %) N content [4–8].

The expansion caused by the interstitial nitrogen in the expanded austenite layer generates compressive lattice strains, which result in a increase in the stacking fault density. Another consequence of nitrogen supersaturation is relating to crystallography of the S phase that yields an anomalous behavior in the x-ray diffraction (XRD) analysis [8–13]. The XRD patterns present peaks with anisotropic shift to lower

Manuscript received November 10, 2010; accepted for publication November 14, 2011; published online December 2011.

¹Dept. of Mechanical and Materials Engineering, Portland State Univ., P.O. Box 751, Portland, OR, 97207-0751, e-mail: GETotten@aol.com

²Dept. of Materials, Aeronautical and Automotive Engineering, São Carlos School of Engineering, Univ. of São Paulo, Av. Trabalhador São-carlense, n. 400, 13566-590, São Carlos, SP, Brazil, e-mail: castelet@sc.usp.br

³Dept. of Materials, Aeronautical and Automotive Engineering, São Carlos School of Engineering, Univ. of São Paulo, Av. Trabalhador São-carlense, n. 400, 13566-590, São Carlos, SP, Brazil, e-mail: codoico@gmail.com

⁴Dept. of Mechanical Engineering, São Paulo State Univ., UNESP – Campus of Ilha Solteira, Av. Brasil Centro, n. 56, 15385-000, Ilha Solteira, SP, Brazil (Corresponding author), e-mail: gallego@dem.feis.unesp.br

Copyright © 2012 by ASTM International, 100 Barr Harbor Drive, PO Box C700, West Conshohocken, PA 19428-2959.

TABLE 1—Nominal chemical composition of stainless steels (wt %).

Steel	C	Mn	P	S	Si	Cr	Ni	Mo	N
S31600	<0.08	<2.0	<0.045	<0.03	<0.75	16.0–18.0	10.0–14.0	2.0–3.0	<0.1
S31254	<0.02	<1.0	<0.030	<0.01	<0.80	19.5–20.5	17.5–18.5	6.0–6.5	0.18–0.22

Bragg angles than those expected for austenite, which promote different expansion among diffracted reflections. Thus {200} peak shows expanded austenite lattice larger than {111} reflection. As a consequence, the elastic distortion of austenite lattice combined with massive stacking fault result in broader and asymmetric XRD peaks, which became hard to identify phases with very small volume fraction, as chromium or iron nitrides nucleated in expanded austenite layer.

In this work plasma nitriding was carried out at different temperatures on austenitic and superaustenitic stainless steels in order to study the microstructural changes after nitriding at 400 °C, 450 °C, and 500 °C. XRD analysis has confirmed that expanded austenite was formed on nitrided layers, but only transmission electron microscopy was able to identify fine precipitation of chromium nitride. The formation of these particles was attributed to localized decomposition of expanded austenite during nitriding treatment.

Materials and Methods

Samples of austenitic UNS S31600 (AISI 316 ASS) and superaustenitic UNS S31254 (254-SMO SASS) stainless steels were prepared starting from rolled bars. Table 1 presents the nominal chemical compositions of the investigated steels. After machining of the disks with 20 mm of diameter and 3 mm of thickness, the surface of the pieces was wet ground and polished. During nitriding processing the pressure of the gaseous mixture of 80 % H₂ and 20 % N₂ (v/v) and the time of treatment were standardized in 500 Pa and 5 h, respectively. The temperatures used for nitriding were 400 °C, 450 °C, and 500 °C. Temperature was monitored using K-type thermocouple. Other details of the nitriding processing were described in previous work [14].

The nitrided samples were analyzed by optical microscopy in a Zeiss Axiotech microscope, equipped with high resolution image acquisition device. Acqua Regia etchant was used to reveal the contrast of the microstructure on the polished surface. Vickers microhardness measurements were made with Buehler digital equipment, where a load of 25 gf (245 mN) was applied during 10 s. The phase characterization in the nitrided layer was accomplished by x-ray diffraction (XRD) in a Rigaku Gergerflex diffractometer equipped with copper tube ($K\alpha_1 = 1.5405 \text{ \AA}$) and graphite monochromator. The diffracted intensity was

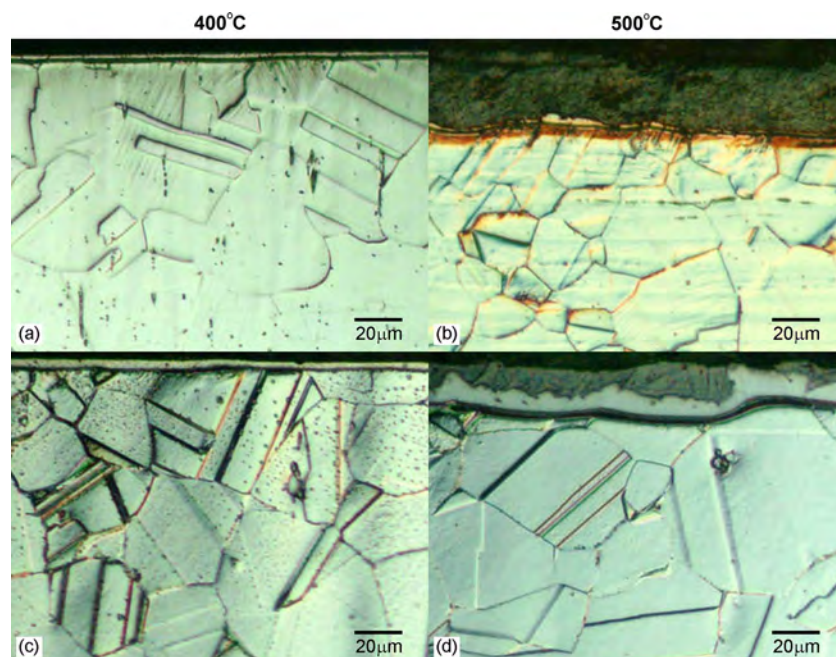


FIG. 1—Optical micrographs showing layer thickness with increasing nitriding temperature from 400 °C to 500 °C. Samples of stainless steels UNS S31600 in (a) and (b) and UNS S31254 in (c) and (d). Etching: *acqua regia*.

registered in the range between 30 and 100 deg, swept with speed of 2 deg/min. Disks with 3.0 mm in diameter were punched from a nitrided layer of UNS S31600 ASS treated at 450 °C for preparing of plan view thin foil TEM samples, where the electron beam is normal to the nitrided surface. The nitrided layer of punched disks was protected with transparent lacquer before substrate-side jet electropolishing. The aim of the lacquer was to protect the treated surface of the sample from the electrolyte during electropolishing that was performed on a Struers Tenupol device using 5 % perchloric acid/95 % acetic acid solution at room temperature with 40 V/45 mA. The TEM observation was carried out in a Philips CM120 microscope operated at 120 kV ($\lambda = 0.0335 \text{ \AA}$). Selected area electron diffraction patterns (SAED) have been analyzed from digital images using a standard calibrated camera length ($\lambda L = 36.4 \text{ \AA mm}$) [15].

Results and Discussion

Optical Microscopy and Microhardness

Figure 1 presents the typical aspect of the nitrided layers in the UNS S31600 and UNS S31254 stainless steels after treatments carried out at 400 °C and 500 °C during 5 h. It is possible to observe that austenitic

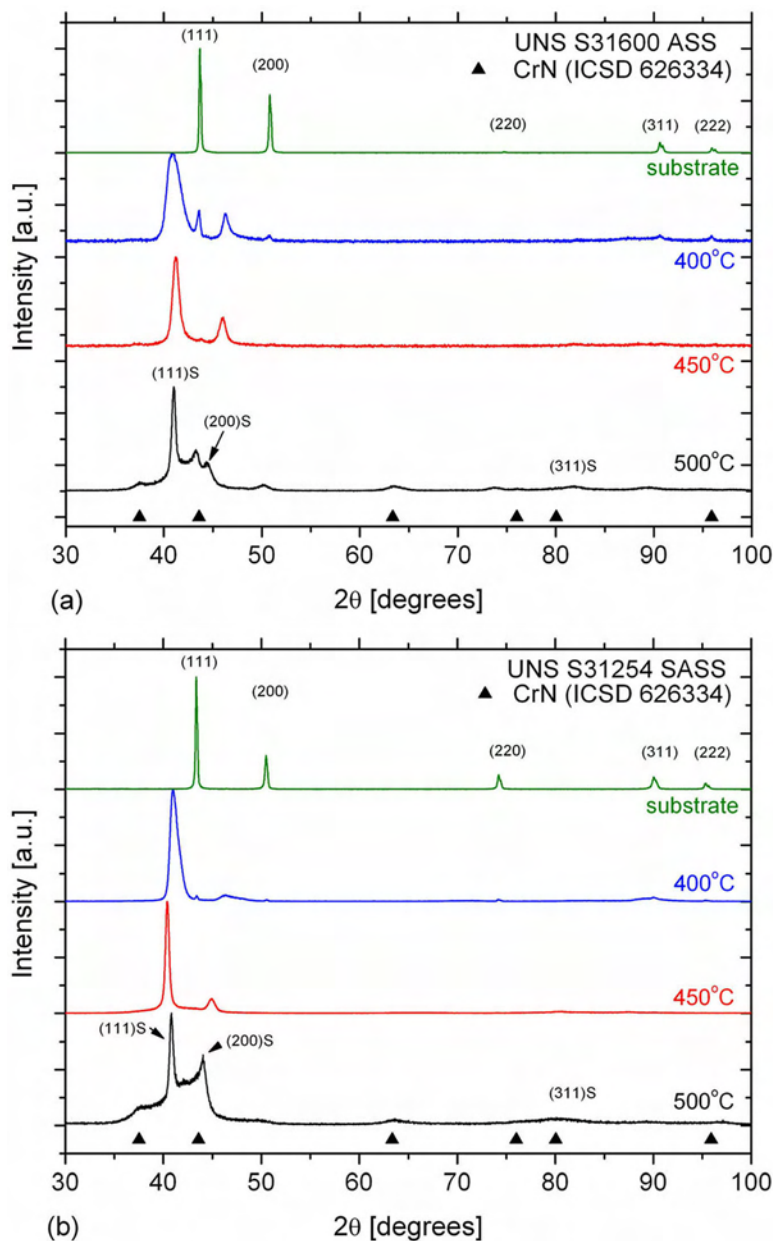


FIG. 2—XRD patterns of the substrate and of the samples nitrided at 400 °C –500 °C. (a) UNS S31600 and (b) UNS S31254 stainless steel.

substrate is composed of grains with polygonal morphology, size close to 40 μm , and many of them showing characteristic annealing twins. The thickness of the nitrided layers increased with the increment of the treating temperature. At 400 °C it has just observed the presence of a thin and homogeneous white layer ($\sim 4 \mu\text{m}$) of expanded austenite in both steels, while in the samples nitrided at 500 °C heterogeneous layers have been observed with thickness between 22 and 26 μm . The nitride formation began on the surface of the samples nitrided at 450 °C, growing in direction to the substrate. The analyses made by optical microscopy have shown that the layers possess regular thickness and that there was no significant difference among them in the investigated steels.

The microhardness measurements have indicated that nitrided layers are much harder than the substrate and the hardness of nitrided layers in the UNS S31600 and UNS S31254 steels have ranged between 850 and 1400 $\text{HV}_{0.025}$. This variation can be associated to the heterogeneity of these layers, because the dispersion of the expanded austenite and nitrides was not uniform starting from 450 °C. The presence of microcavities probably resulted from nitriding processing and the increase of the fragility in the nitrided layers favored the microcracking formation, which can cause variations in the microhardness measurements. The mean hardness of the substrate was 175 $\text{HV}_{0.025}$ for UNS S31600 and 250 $\text{HV}_{0.025}$ for UNS S31254, respectively. This difference was attributed to the presence of larger amounts of alloying elements (Cr, Ni, and Mo) in the superaustenitic stainless steel that are responsible by solid solution strengthening of the metallic matrix.

XRD Analysis

The XRD patterns are presented in Fig. 2. They show that new phases were formed on the surface of the nitrided steels at higher nitriding temperature. Considering the limited penetration of the x rays in the ferrous alloys due to absorption and the thickness of the nitrided layer, it is quite probable that all diffracted intensity is just coming from these layers. The investigated steels have different amounts of substitutional alloying elements such as chromium, nickel, and molybdenum (Table 1). The amount of nitrogen in the S31254 SASS is larger than the existent in the S31600 ASS. In spite of this variation in the chemical composition, a significant change was not verified in the 2-theta positioning of the main reflections {111} and {200} of the fcc crystalline lattice of nontreated austenite, as indicated in Fig. 2. That is due to the Bragg diffraction angle being sensitive to the lattice parameter (i.e., the atomic position), while the intensity is

TABLE 2—Austenite-based XRD data ($\text{Cu } K_{\alpha}$) extracted from literature, where are indicated the average (AVG) and standard deviation (SD) of 2θ angle from (hkl) reflection, the full width at half maximum (FWHM), the width of the peak base (FW-base), the interplanar spacing $d(\text{hkl})$ of the lattice parameter (a_o^i), and its relative lattice expansion (% exp), calculated from Eq 1.

(hkl) ^a		2θ (deg)	FWHM (deg)	FW-Base (deg)	$d(\text{hkl})$ (Å)	a_o^i (Å)	% exp
(111)S	AVG	41.1777	1.2860	3.0466	2.1913	3.7954	5.69
	SD (46)	0.8259	0.5290	1.1415	0.0422	0.0732	2.04
(111)	AVG	43.5745	0.9714	2.6713	2.0754	3.5947	0.10
	SD (42)	0.3003	1.0275	3.1161	0.0136	0.0235	0.65
(200)S	AVG	46.9166	1.4348	3.8821	1.9361	3.8722	7.83
	SD (46)	1.1488	0.7608	2.4367	0.0446	0.0893	2.49
(200)	AVG	50.6816	0.5641	1.3619	1.7998	3.5995	0.23
	SD (33)	0.2774	0.2336	0.6686	0.0093	0.0186	0.52
(220)S	AVG	70.2533	1.8348	4.4994	1.3399	3.7899	5.54
	SD (13)	2.2531	0.6669	2.0417	0.0378	0.1069	2.98
(220)	AVG	74.6885	0.7375	1.6826	1.2698	3.5916	0.01
	SD (13)	0.1734	0.3206	0.7685	0.0025	0.0071	0.20
(311)S	AVG	83.4144	2.1240	5.2925	1.1585	3.8422	6.99
	SD (13)	2.2647	1.0719	2.1096	0.0245	0.0813	2.27
(222)S	AVG	86.9261	2.4406	7.0076	1.1198	3.8792	8.02
	SD (7)	0.6626	0.5344	1.2675	0.0068	0.0237	0.66
(311)	AVG	90.6261	0.6864	1.6731	1.0834	3.5934	0.06
	SD (10)	0.0961	0.2017	0.4709	0.0009	0.0030	0.08
(222)	AVG	95.9937	0.6022	1.6849	1.0366	3.5908	-0.01
	SD (4)	0.0683	0.1089	0.6446	0.0006	0.0019	0.05

^aThe numbers between parentheses together with SD represent the number of results used for statistics.

affected by the atomic number of the atom in the lattice positions [5,8,11]. The intensity variation can be explained due to random occupation of the lattice points by different alloying elements (substitutional and interstitial) and the effect of texture, introduced by the plastic deformation of the rolled bars. The {220} austenite peak in those steels was attenuated by the last reason.

The 2-theta position of several reflections observed in the XRD results showed in Fig. 2 does not match with cards classified in the main diffraction databases, like JCPDS-ICDD (International Centre for Diffraction Data) or ICSD (Inorganic Crystal Structure Database). The expanded austenite phase is thermodynamically metastable and has commonly been observed in nitrided layers. In Fig. 2 the letter “S” identifies its (hkl) reflections. To help the identification of diffracted peaks of this phase Table 2 was elaborated, based on an extensive bibliographical revision regarding data of expanded austenite obtained by XRD (not completely cited here). Table 2 presents average values (AVG) of the 2-theta angle of reflection, the full width at half maximum (FWHM), the width of the peak base (FW-base), the interplanar spacing $d(hkl)$ calculated by Bragg’s law, the lattice parameter a_o^i of the i phase, and the relative lattice expansion (% exp) calculated for

$$\% \text{ exp} = \left(\frac{a_o^i - a_o}{a_o} \right) \times 100 \quad (1)$$

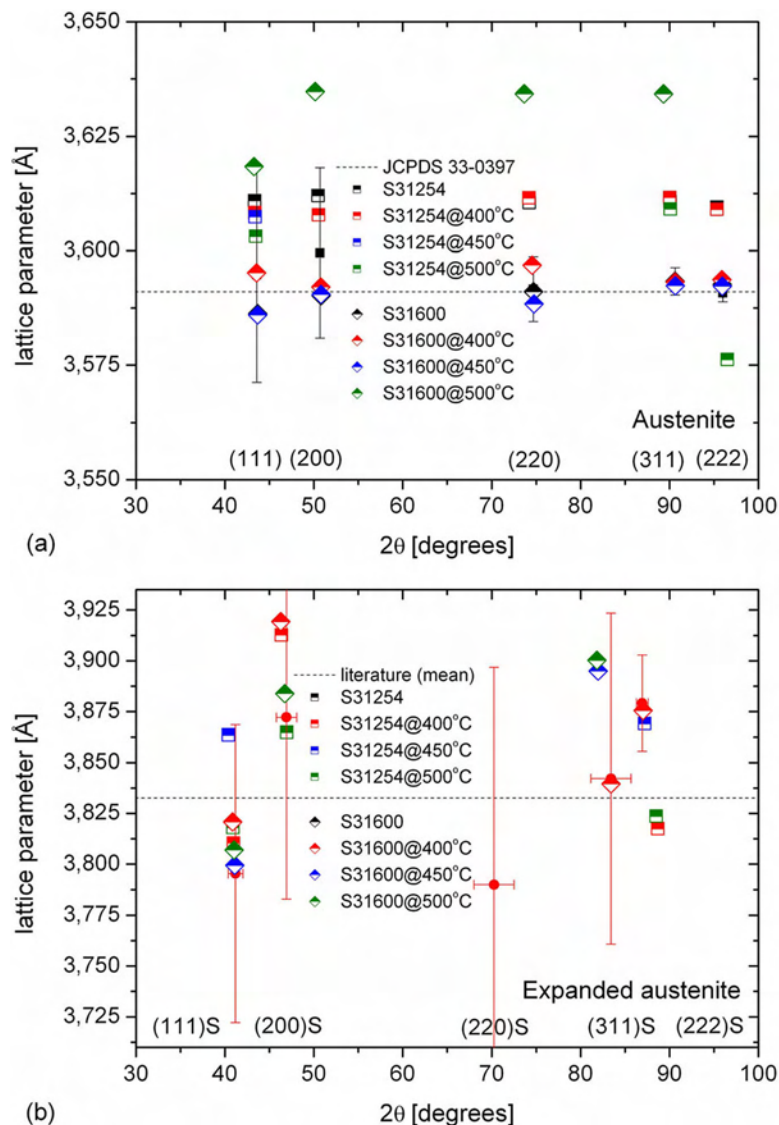


FIG. 3—Lattice parameter from austenite (a) and expanded austenite (b) calculated from XRD pattern of Fig. 2. Here dispersion is being represented by standard deviation of the results collected from the literature (see Table 2).

In Eq 1 a_o is the lattice parameter of the austenite (35911 Å) in #33-0397 JCPDS card. The term “SD” represents the standard deviation of data and the number inside parentheses indicates the amount of peaks collected from the literature.

The experimental XRD results of calculated lattice parameter for both steels have showed good fitting with those listed in Table 2, whose illustration is shown in Fig. 3. The lattice expansion has changed depending on the (hkl) reflection. The results from “normal” austenite peaks do not overcome 1% of respective JCPDS card [Fig. 3(a)], but there are significant increasing (higher than 10%) in the expanded austenite lattice when the (200)S reflection is considered [Fig. 3(b)]. For (111)S peaks this enlargement was smaller, varying from 4.7 to 6.5%. The presence of the expanded austenite is characterized in the XRD patterns by broadened peaks (higher FWHM) that are shifted for diffraction angles smaller those observed for the normal austenite. Besides this, the displacement of diffracted peaks is anomalous because the cubic lattice parameter calculated for the (200)S reflection is significantly larger than those obtained for other reflections. This behavior is not still completely understood [9] but certainly is related to the introduction of a massive amount of nitrogen in the austenite. The N concentration in expanded austenite can reach nearly 40 at %, higher than its limit of solubility in the austenite (10.3 at %) [16]. The occupancy of the octahedral positions in the fcc lattice increases as the concentration of nitrogen rises. The anisotropic diffusion of the interstitial [4], the presence of chromium and molybdenum [17], and the probable increase of stacking fault density, promoted by decreasing of its energy formation due to the presence of nitrogen [13], generate elastic distortion in the crystal lattice of austenitic matrix, which is responsible by diffracted peaks broadening observed in the XRD analysis of expanded austenite.

Nitriding temperature and chromium take important roles in controlling of nitrogen diffusion and stabilization of expanded austenite. The effect of temperature on the lattice expansion is illustrated in Fig. 4, which shows that distortion was higher after plasma nitriding of UNS S31600 ASS at 450 °C. The larger amount of nitrogen in the UNS S31254 SASS has not probably contributed to increasing the lattice size. In the same graph it is possible to verify the effect of anomalous lattice distortion with different (hkl) reflections. Lower lattice expansion determined at 400 °C and 500 °C can be associated, respectively, to decrease of nitrogen diffusivity into the austenitic matrix and the formation of chromium (most probably) or iron (less probably) nitrides, whose effects reduce nitrogen supersaturation. The random dispersion of chromium atoms in the matrix, allied with the strong chemical affinity with nitrogen and low diffusion rates, has enhanced the implantation of the interstitial in austenite where it acts as a “nitrogen trapping” [6]. In lower nitriding temperatures, in spite of the supersaturation and its smaller standard free energy of formation [18], it should not have intense chromium nitride nucleation. These nitrides are just formed in higher temperatures and times of nitriding by thermodynamic and kinetics reasons [6], as can be observed

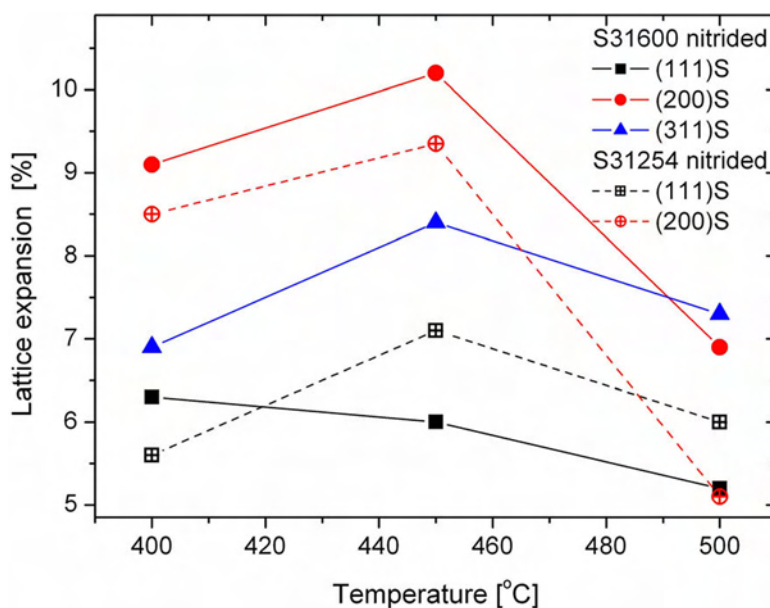


FIG. 4—Effect of temperature on the lattice expansion estimated from different reflections of expanded austenite in UNS S31600 and UNS S31254 stainless steels.

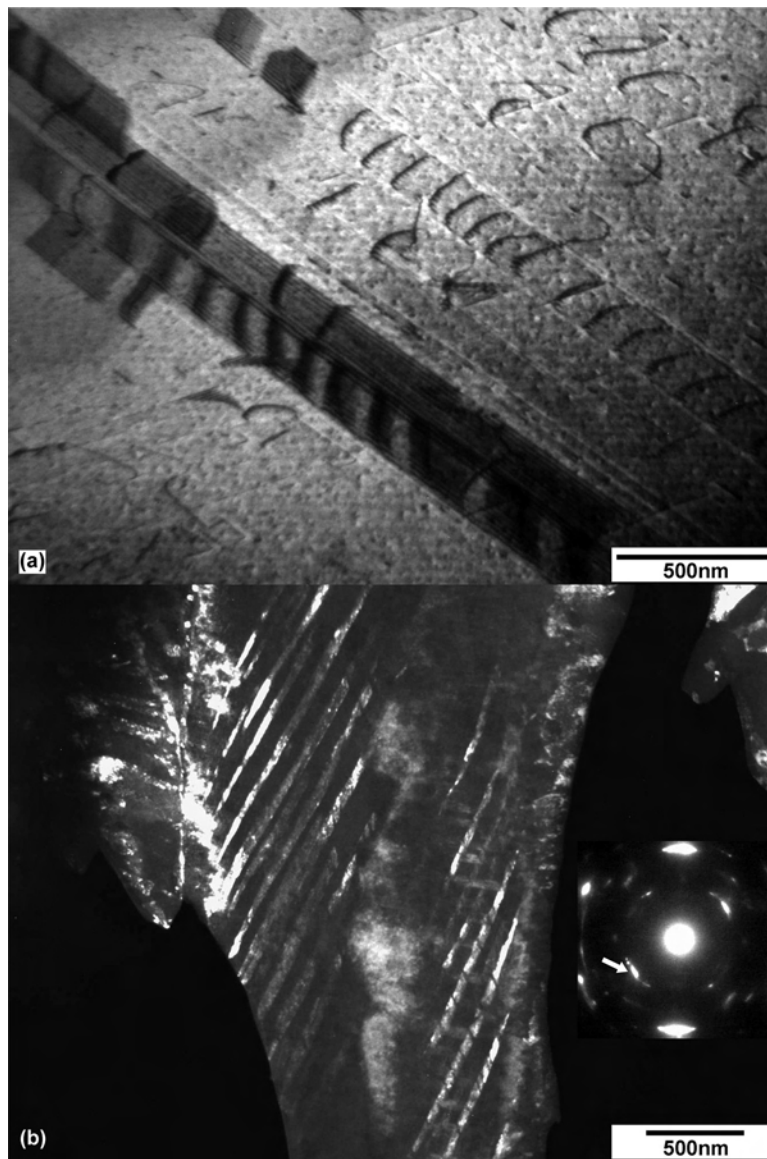


FIG. 5—Thin foil BF TEM micrograph showing planar distribution of dislocations in (a). A bundle of stacking faults revealed by selection of (111) reflection of UNS S31600 stainless steel is showed in (b).

from XRD pattern obtained after nitriding at 500 °C (Fig. 2). However, XRD analysis is not the most indicated technique to investigate phases with very small volume fraction.

TEM Analysis

The observation of thin foils by TEM have verified the typical presence of dislocations and stacking faults in the UNS S31600 steel substrate, as shown, respectively, by the micrographs from Fig. 5. All crystalline defects increase the mobility of the nitrogen, favoring the insertion and the diffusion of the interstitial element in the austenite [11]. The analysis of different regions by selected area electron diffraction (SAED) have systematically showed well defined spot-type patterns, characteristic of reflections of fcc austenite monocrystals with lattice parameters quite close to that determined for the substrate by XRD ($\approx 3.60 \text{ \AA}$).

The bright field TEM micrograph of Fig. 6 exhibits a plan view section on the nitrided surface where three grains of expanded austenite and its respective SAED patterns are presented. The electron diffraction analysis shows that each grain maintained the fcc structure with different zone axes. Calculations involving measurements from these patterns allow estimating an expansion of the lattice parameter up to 14.5 %, as show Table 3. According to Christiansen and Somers [19], the maximum expansion obtained is 11.2 %, but this difference can be associated with very small thickness ($< 100 \text{ nm}$) of the observation area in TEM samples. Meletis and colleagues [20] reported that compressive nitriding-induced residual stresses are

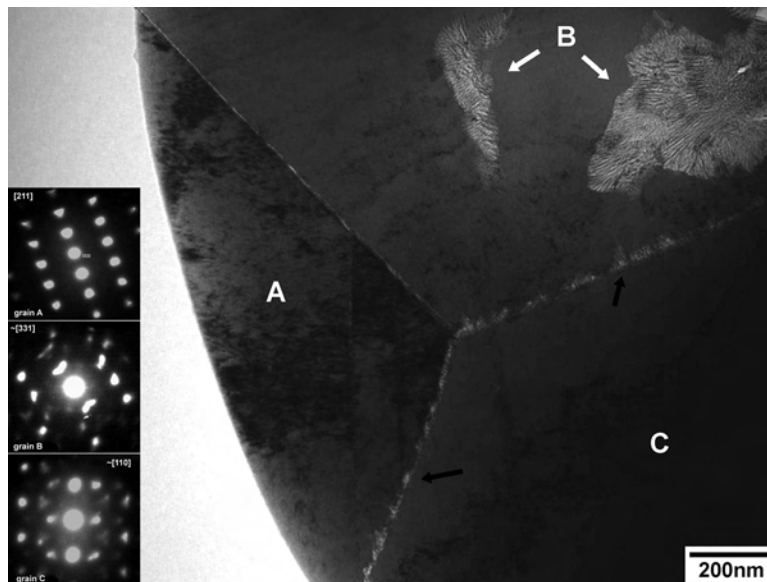


FIG. 6—Plan view thin foil BF TEM image showing grains of expanded austenite and their respective SAED patterns. Some phase decomposition regions are indicated on B grain surface (white arrows) and in the grain boundaries (black arrows).

much lower in thin foil than bulk specimens, which is consistent with larger lattice parameters of expanded austenite calculated from SAED patterns.

The scatter of reported results presented in Table 3 can be associated with the broadening of diffracted spots due to the nitrogen-supersaturated solid solution that usually shows diffuse rel-rods intensity in the SAED patterns [15]. It is possible that there were different N concentrations in each grain, resulting from anisotropic diffusion of interstitial [4]. Here it is important to highlight that {200} reflections have presented in Table 3 an anomalous behavior, similar to the one verified previously by XRD in Fig. 4. In the same micrograph it is possible to identify “colonies” (marked with white arrows in Fig. 6) on the surface of the grain “B” whose morphology is quite similar to that observed in nitrated layers investigated by Mitchell et al. [21] and Xu and colleagues [22]. These colonies result from localized expanded austenite decomposition and they display a lamellar type microstructure composed by ferrite and cubic chromium nitride [13,21]. This decomposition mechanism is probably controlled by the atomic diffusion of the chromium that is very sluggish at 450 °C. Thus, only chromium rich regions would be capable for the transformation, where the precipitation of CrN would reduce drastically the stability of the austenite promoted by the interstitial (N is considered a very strong austenite former). Evidence of expanded austenite decomposition were also observed on the grain boundaries, as indicated by black arrows in Fig. 6.

Besides provoking the formation of diffuse spots in the SAED patterns, the massive introduction of nitrogen caused an extensive twinning in the expanded austenite due to high elastic strain associated with interstitial supersaturation. These features were usually observed in a set of bundles, as exemplified by

TABLE 3—SAED data from various orientations of the grains showed in Fig. 6.

Grain	$d(hkl)$ (Å)	h	k	l	a_o (Å)	% exp (%)
A	2.233	1	1	1	3.868	7.7
C	2.056	2	0	0	4.112	14.5
B	2.045	2	0	0	4.090	13.9
C	1.400	2	2	0	3.960	10.3
A	1.363	2	2	0	3.855	7.4
B	1.185	3	1	1	3.930	9.4
A	1.167	3	1	1	3.871	7.8
C	1.152	2	2	2	3.991	11.1
B	0.888	4	2	0	3.971	10.6
C	0.886	4	2	0	3.962	10.3

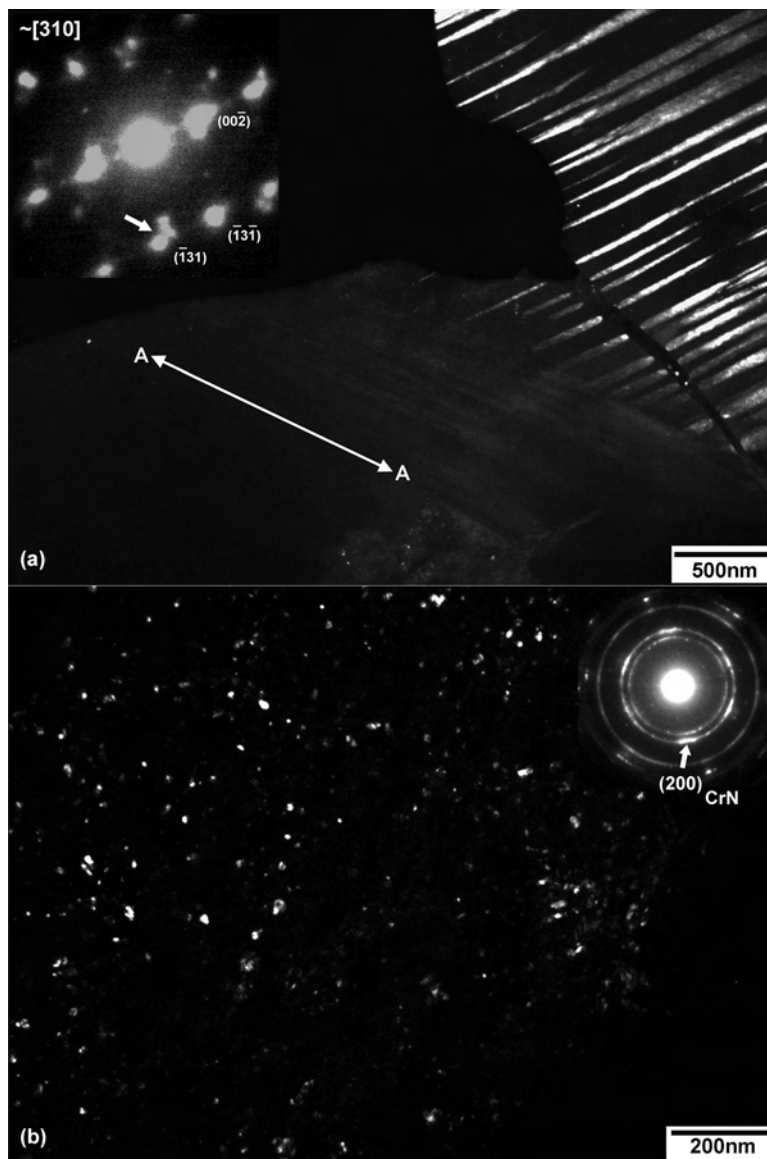


FIG. 7—Thin foil dark field micrographs showing two sets of stacking faults in (a) and 10–15 nm size rounded nitride particles found after plasma nitriding of UNS S31600 stainless steel at 450 °C in (b). The selected reflections for imaging are indicated in the respective SAED patterns.

dark field TEM micrograph of Fig. 7(a) where low contrast of stacking faults in A-A direction is due to very closed diffracted beams selected by the objective aperture of TEM (see white arrow). In some regions of the nitrided layer small rounded particles (10–15 nm) were found, as showed in Fig. 7(b). The ring-type SAED pattern indicates that there is a larger number of diffracting particles and there is also a preferential orientation (texture) relating substrate, not investigated here. Indexing diffracted rings have showed that these particles possess a crystalline structure compatible with cubic chromium nitride (CrN), whose volume fraction is considerably smaller than the detection limit of the XRD technique.

XRD and TEM were applied in the characterization of expanded austenite in nitrided layers. Both techniques were able to show that the austenite lattice does not expand uniformly, where expansion along $\langle 100 \rangle$ is larger than that $\langle 111 \rangle$. Explanations for that still needs further investigation.

Conclusions

- The variation of the nitriding temperature has caused changes in the thickness and on the microstructure of the nitrided layers on UNS S31600 and UNS S31254 steels.
- The formation of expanded austenite in the nitrided layers from 400 °C to 500 °C was confirmed by XRD analyses that show its “anomalous” lattice expansion up to 10 %, resulting from colossal

nitrogen supersaturation. The maximum lattice expansion in both steels has been observed when plasma nitriding temperature was 450 °C.

- The observation of UNS S31600 nitrided samples by TEM have showed that cubic CrN forms at 450 °C, but it could not be identified by XRD analysis due to its small volume fraction. Chromium nitride probably resulted from localized expanded austenite decomposition during nitriding treatment.

Acknowledgments

The writers would like to thank Brazilian research agencies CNPq (L.C.C. and J.G.) and CAPES (F.A.P.F.) for received grants.

References

- [1] Bell, T., Mao, K., and Sun, Y., "Surface Engineering Design: Modelling Surface Engineering Systems for Improved Tribological Performance," *Surf. Coatings Technol.*, Vol. 108–109, 1998, pp. 360–368.
- [2] Zhu, X., Huang, H., Xu, K., and He, J., "Structure and Properties of Plasma Nitrided Austenitic Stainless Steel," *20th ASM Heat Treating Soc. Conf. Proc.*, Vol. 1–2, 2000, pp. 217–221.
- [3] Menthe, E., Rie, K.-T., Schultze, J. W., and Simson, S., "Structure and Properties of Plasma Nitrided Stainless Steel," *Surf. Coatings Technol.*, Vol. 74–75, 1995, pp. 412–416.
- [4] Rivière, J. P., Templier, C., Declémy, A., Redjda, O., Chumlyakov, Y., and Abrasonis, G., "Microstructure of Expanded Austenite in Ion-Nitrided AISI 316L Single Crystals," *Surf. Coatings Technol.*, Vol. 201, 2007, pp. 8210–8214.
- [5] Christiansen, T. and Somers, M. A. J., "On the Crystallographic Structure of S-Phase," *Scr. Mater.*, Vol. 50, 2004, pp. 35–37.
- [6] Williamson, D. L., Ozturk, O., Wei, R., and Wilbur, P. J., "Metastable Phase Formation and Enhanced Diffusion in f.c.c. Alloys Under High Dose, High Flux Nitrogen Implantation at High and Low Ion Energies," *Surf. Coatings Technol.*, Vol. 65, 1994, pp. 15–23.
- [7] Sozinov, A. L., Balanyuk, A. G., and Gavriljuk, V. G., "N–N Interaction and Nitrogen Activity in the Iron Base Austenite," *Acta Mater.*, Vol. 47, 1999, pp. 927–935.
- [8] Christiansen, T. L., Hummelshøj, T. S., and Somers, M. A. J., "Expanded Austenite, Crystallography and Residual Stress," *Surf. Eng.*, Vol. 26, 2010, pp. 242–247.
- [9] Dong, H., "S-Phase Surface Engineering of Fe–Cr, Co–Cr and Ni–Cr Alloys," *Int. Mater. Rev.*, Vol. 55, 2010, pp. 65–98.
- [10] Buhagiar, J., Li, X., and Dong, H., "Formation and Microstructural Characterisation of S-Phase Layers in Ni-Free Austenitic Stainless Steels by Low-Temperature Plasma Surface Alloying," *Surf. Coatings Technol.*, Vol. 204, 2009, pp. 330–335.
- [11] Manova, D., Eichentopf, I.-M., Hirsch, D., Mändl, S., Neumann, H., and Rauschenbach, B., "Influence of Microstructure on Nitriding Properties of Stainless Steel," *IEEE Trans. Plasma Sci.*, Vol. 34, No. 4, 2006, pp. 1136–1140.
- [12] Li, X.Y., "Low Temperature Plasma Nitriding of 316 Stainless Steel-Nature of "S" Phase and Its Thermal Stability," *Surf. Eng.*, Vol. 17, No. 2, 2001, pp. 147–152.
- [13] Xu, X. L., Wang, L., Yu, Z.W., and Hei, Z. K., "Microstructural Characterization of Plasma Nitrided Austenitic Stainless Steel," *Surf. Coatings Technol.*, Vol. 132, 2000, pp. 270–274.
- [14] Fernandes, F. A. P., Heck, S. C., Pereira, R. G., Picon, C. A., Nascente, P. A. P., and Casteletti, L. C., "Ion Nitriding of a Superaustenitic Stainless Steel: Wear and Corrosion Characterization," *Surf. Coatings Technol.*, Vol. 204, 2010, pp. 3087–3090.
- [15] Williams, D. B. and Barry Carter, C., *Transmission Electron Microscopy: A Textbook for Materials Science*, Springer Science and Business Media, New York, 2009, 760 pp.
- [16] Raghavan, V., "The Cr-Fe-N-Ni System," *J. Phase Equilibria*, Vol. 18, No. 2, 1997, pp. 158–172.
- [17] Li, X., Samandi, M., Dunne, D., and Hutchings, R., "Evolution of the Microstructure of Austenitic Stainless Steel Nitrogen Implanted at Elevated Temperatures," *Surf. Coatings Technol.*, Vol. 71, 1995, pp. 175–181.

- [18] He, Y., Li, Z., Qi, H., and Gao, W., “Standard Free Energy Change of Formation Per Unit Volume: A New Parameter for Evaluating Nucleation and Growth of Oxides, Sulphides, Carbides and Nitrides,” *Mater. Res. Innovation*, Vol. 1, 1997, pp. 157–160.
- [19] Christiansen, T. L. and Somers, M. A. J., “Controlled Dissolution of Colossal Quantities of Nitrogen in Stainless Steel,” *Metallurg. Mater. Trans. A*, Vol. 37A, 2006, pp. 675–682.
- [20] Meletis, E. I., Singh, V., and Jiang, J. C., “On the Single Phase Formed During Low-Temperature Plasma Nitriding of Austenitic Stainless Steels,” *J. Mater. Sci. Lett.*, Vol. 21, 2002, pp. 1171–1174.
- [21] Mitchell, D. R. G., Attard, D. J., Collins, G. A., and Short, K. T., “Characterisation of PI3 and RF Plasma Nitrided Austenitic Stainless Steels Using Plan and Cross-Sectional TEM Techniques,” *Surf. Coatings Technol.*, Vol. 165, 2003, pp. 107–118.
- [22] Xu, X., Wang, L., Yu, Z., Qiang, J., and Hei, Z., “Study of Microstructure of Low-Temperature Plasma-Nitrided AISI 304 Stainless Steel,” *Metallurg. Mater. Trans. A*, Vol. 31A, 2000, pp. 1193–1199.